

J. Einarsson · A. Johansson · S.K.
Mahato · Y.N. Mishra · J.R. Angilella ·
D. Hanstorp · B. Mehlig

Aperiodic tumbling of microrods advected in a microchannel flow

Received: date / Accepted: date

Abstract We report on an experimental investigation of the tumbling of microrods in the shear flow of a microchannel (dimensions: $40\text{ mm} \times 2.5\text{ mm} \times 0.4\text{ mm}$). The rods are $20\text{ }\mu\text{m}$ to $30\text{ }\mu\text{m}$ long and their diameters are of the order of $1\text{ }\mu\text{m}$. Images of the centre-of-mass motion and the orientational dynamics of the rods are recorded using a microscope equipped with a CCD camera. A motorised microscope stage is used to track individual rods as they move along the channel. Automated image analysis determines the position and orientation of a tracked rods in each video frame. We find different behaviours, depending on the particle shape, its initial position, and orientation. First, we observe periodic as well as aperiodic tumbling. Second, the data show that different tumbling trajectories exhibit different sensitivities to external perturbations. These observations can be explained by slight asymmetries of the rods. Third we observe that after some time, initially periodic trajectories lose their phase. We attribute this to drift of the centre of mass of the rod from one to another stream line of the channel flow.

Keywords Microrods · microchannel · Jeffery orbits · tumbling

1 Introduction

It was shown by Jeffery (1922) that small axisymmetric rods in a viscous shear flow align for the most time with the flow direction, but that their symmetry axes periodically and rapidly turn by 180 degrees. This motion is referred to as ‘tumbling’ in the literature. Experimental studies of tumbling of

J. Einarsson · A. Johansson · S.K. Mahato · Y.N. Mishra · D. Hanstorp · B. Mehlig
Department of Physics, University of Gothenburg, 412 96 Gothenburg, Sweden

J. R. Angilella
LUSAC, Université de Caen, Cherbourg, France

particles in flows have been performed for a long time, see for example (Goldsmith and Mason, 1962). More recently, Kaya and Koser (2009) performed an experiment analysing the tumbling of *E. coli* cells in microchannel shear flows. They characterised the tumbling by fitting periodic orientational trajectories to short experimental time series. A similar approach was adopted by Mishra et al. (2012) to describe the tumbling of microrods in a microchannel flow. The periodic solutions referred to above were first obtained by Jeffery (1922) and are commonly referred to as ‘Jeffery orbits’.

Hinch and Leal (1979) have shown by theoretical analysis that slightly asymmetric rods also tumble, but that their orientational motion is in general not strictly periodic. Under certain circumstances the authors predict that the orientational dynamics may be ‘doubly periodic’. Yarin et al. (1997) refer to this motion as ‘quasi periodic’. Their numerical results show that the tumbling can be chaotic (Ott, 1993). In order to experimentally distinguish periodic from aperiodic tumbling due to asymmetry, it is necessary to observe long sequences of flips. A confounding factor is rotational and centre-of-mass diffusion: the centre of mass of an advected rod may diffuse to neighbouring stream lines of the flow. This causes aperiodicity. But noise can also directly affect the rotational degrees of freedom, leading to random tumbling.

In order to disentangle these effects it is necessary to follow the orientational dynamics for many flips. The rods must therefore be tracked for long distances. To achieve this we have improved an existing experimental setup (Mishra et al., 2012) in two ways. First, we have automated the image analysis of the empirical data. Second, with the new setup it is possible to periodically revert the channel flow. This allows us to record longer tumbling sequences. In an ideal experiment the orientational dynamics is expected to retrace its trajectory upon reversal of the flow. This is a consequence of the time-reversal invariance of the Stokes equation governing low Reynolds-number flow. Our setup thus enables us to quantify the sensitivity of the observed tumbling motion to perturbations. In the following we report and discuss experimentally observed tumbling trajectories. First, we see periodic and aperiodic tumbling. Second, different tumbling trajectories exhibit different sensitivities to external perturbations. We argue that these observations can be explained by slight asymmetries of the rods. Third, at very long times initially periodic trajectories lose their phase. We attribute this to drift of the centre of mass of the rod from one to another stream line of the channel flow.

We conclude this introduction by briefly commenting on the relevance of the questions addressed in this paper. Jeffery’s periodic tumbling solutions in shear flows form, together with orientational diffusion, the basis of many studies of the rheology of suspensions of non-spherical particles, as outlined by Hinch and Leal (1972). Petrie (1999) has given an overview over the rheology of fibre suspensions and the use of Jeffery’s and diffusion theory in this field. Furthermore, pattern formation by non-spherical particles in random flows was investigated using Jeffery’s theory by Wilkinson et al. (2009) and Bezuglyy et al. (2010) (see also Wilkinson et al. (2011)), identifying singularities in the orientational patterns of rheoscopic suspensions, and explaining how Jeffery’s periodic solutions determine rheoscopic visualisations of flows.

Last but not least, the tumbling and alignment of small rods in turbulent flows has recently been intensively investigated, both experimentally, by simulations, and theoretically. We refer to the articles in this special issue of *Acta Mechanica*, as well as to (Parsa et al., 2012) and (Wilkinson and Kennard, 2012) and articles cited in these two papers. Simulations and the theoretical treatments of the tumbling of small rods in turbulent flows are based on Jeffery's equation of motion.

2 Materials & methods

In summary, the microrods are produced by means of a liquid-liquid dispersion technique (Alargova et al., 2004). They are introduced into a microchannel system produced in PDMS. The flow is pressure-driven, using a syringe pump. The flow direction is periodically reverted. The fluid is a 2:1 mixture of glycerol to water, so the viscosity is high, and the Reynolds number is low. The centre-of-mass motion and orientation of the microrods are observed using a 20 X microscope equipped with a CCD camera. A motorised stage allows to track individual rods over long time periods. The resulting sequence of frames is analysed by an automated image-analysis algorithm programmed in MATLAB, resulting in the orientational trajectories displayed in Figs. 5 to 7.

2.1 Experimental methods

Particle synthesis. As in our earlier experiments (Mishra et al., 2012), the polymer microrods are prepared by a liquid-liquid dispersion technique using the protocol of Alargova et al. (2004). This method produces rods with lengths of 10 μm to 100 μm , with typical aspect ratios of the order of 10:1. The resolution of the microscope does not allow us to determine whether the rods are symmetric or not, that is, whether they have perfectly circular or slightly elliptical cross sections. Inspection under an optical microscope shows that the shorter rods are straight. Some of the longer rods are curved. In the experiments described below, rods in the shorter range of the span given above are used.

Design and fabrication of microfluidic channels. The microfluidic device used in this experiment is shown schematically in Fig. 1. The channel (40 mm long, 2.5 mm wide, and 0.4 mm deep) is produced in PDMS. The procedure is described in detail by Mishra et al. (2012).

Optical system and tracking. A sketch of the experimental setup is shown in Fig. 1. The optical setup is based on a Nikon Eclipse Inverted Microscope. The channel is placed on a motorised stage, making it possible to track the rods as they follow the flow in the channel. The rods are observed using a 20X microscope objective (NA=0.28). Images are recorded with a CCD camera (Leica DFC 350FX, Switzerland) at a frame rate of 100 frames per second. As shown in Fig. 1, the images are observed through the cover glass. Since the magnification of the microscope is only 20X, the thickness of the

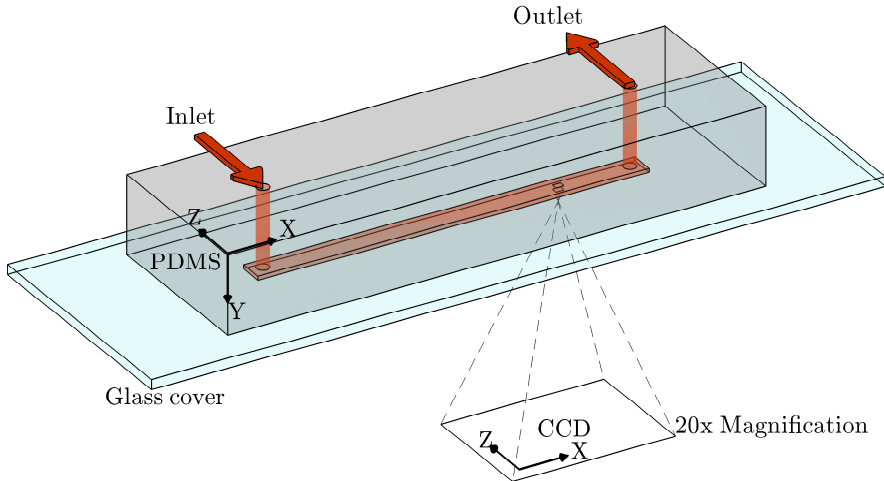


Fig. 1: Experimental setup (schematic) with coordinate system. The microchannel is placed upon a motorised stage which allows the camera to study any part of the channel. The calculated flow rates in a cross-section of the channel are shown in Fig. 2.

glass does not cause focal problems. The channel is illuminated through the transparent PDMS.

Fig. 1 also shows the Cartesian coordinate system adopted in this paper. The x -axis is taken to lie along the flow in the channel. the y -axis lies along the optical axis of the microscope (the channel is $400\ \mu\text{m}$ deep in this direction). The z -axis, finally, lies along the width of the channel (it is $2.5\ \text{mm}$ wide). Thus the camera plane corresponds to the x - z -plane, and the channel cross section (Fig. 2) corresponds to the y - z -plane.

Channel flow. The flow in the microchannel is characterised by a very small Reynolds number. The rods are suspended in a 2:1 mixture of glycerol and water, corresponding to a kinematic viscosity of $\nu = 2 \cdot 10^{-5}\ \text{m}^2/\text{s}$ (Cheng, 2008). The flow speed is of the order of $100\ \mu\text{m}/\text{s}$. Based on the smallest channel dimension ($400\ \mu\text{m}$) this yields a Reynolds number of the order of $\text{Re} = 10^{-3}$. The Navier-Stokes equations for the incompressible flow in the channel thus reduce to the viscous Stokes equation which can be simply solved by a basis expansion. Closely following Brody et al. (1996) we have computed the flow profile in a cross section far from the in- and outlets (so that we can neglect the x coordinate). We assume no-slip boundary conditions at the channel walls and a constant pressure gradient over the channel length. The resulting profile for our channel geometry is shown in Fig. 2. The resulting flow velocity scales as $u_x \sim \Delta p/\eta$ as a function of pressure difference Δp and dynamic viscosity η . But the form of the profile is not affected by the values of Δp or η . In Fig. 2 we observe that close to the centre of the channel, the flow gradient is oriented along the y -axis. In the following we refer to this axis as the ‘shear direction’. The x -axis is termed ‘flow direction’, and the z -axis ‘vorticity direction’.

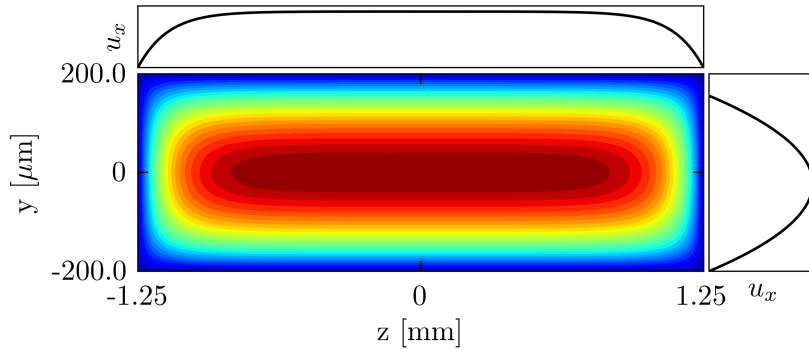


Fig. 2: Computed flow profile for the channel geometry used in experiments. Width (z) of channel is 2.5 mm and depth (y) is 400 μm (refer to Fig. 1 for coordinate system). The intensity plot shows a cross-section of the channel, intensity indicating flow velocity in arbitrary units. Top and right panels show the corresponding flow-velocity profiles at $y = 0$ and at $z = 0$, respectively.

The rods analysed in this paper are between 20 μm to 30 μm long. The viscous time scale L^2/ν is of the order of 10^{-5}s , which is much smaller than both the tumbling and the flow-reversal time scales. The disturbance flow around the inclusion is therefore expected to obey the quasi-steady Stokes equation, in spite of the motion of the rod.

2.2 Data analysis

As explained below, the rods often tumble aperiodically. To classify different dynamical behaviours requires long time series. Since one traversal of the channel takes approximately 5 minutes, large amounts of data must be analysed. We have therefore designed a data analysis software (in MATLAB) to track the centre-of-mass and orientational motion of the suspended rods in an automated fashion.

The raw data from the experiment consist of time-stamped positions of the motorised stage, together with frame sequences from the microscope. The analysis uses this information to estimate time series of the centre-of-mass position of a given rod, and the orientation of the unit vector \mathbf{n} along its major axis:

$$\mathbf{n} = (n_x, n_y, n_z). \quad (1)$$

The coordinate system is shown in Fig. 1.

In the remainder of this section we briefly describe how the empirical data were processed. First, we summarise our algorithm for the image analysis. Second we explain how time is rescaled to account for variations in the flow velocity due to reversals of the direction of the flow and due to fluctuations in the pump pressure.

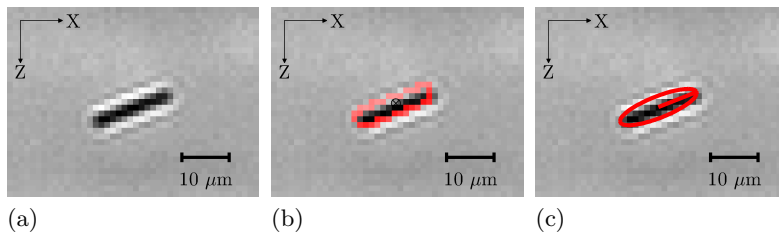


Fig. 3: Three steps of the data analysis. (a) the particle is located within the video frame, (b) edges are detected with an edge-detection algorithm (Canny, 1986), (c) an ellipse is fitted to the resulting edge pixels. The orientation of the major axis of the ellipse is used to estimate orientation of the rod in the camera plane.

2.2.1 Image analysis

The automated image-analysis software tracks the centre of mass and the orientation of a given rod as it moves in the channel. We separately discuss two steps: detecting the position and orientation of the rod, and estimating its length.

Finding the rod position and orientation. To begin with, static image noise is removed as follows. For each pixel, the time-averaged intensity is computed, and for each time, the average intensity of the frame is calculated. Then, for each pixel, the time-averaged intensity is subtracted from the instantaneous intensity, and the instantaneous frame average is added.

To locate the rod in a given frame, the software requires an initial guess of the centre-of-mass position. The frame rate is sufficiently high so that the tracked rods move only slightly between subsequent frames. The initial guess is therefore taken to be the last-known rod position (for the first frame, manual user input is required).

Once the location of the rod within a given frame has been estimated, a smaller window is cropped around the approximate position of the particle. An example is shown in Fig. 3a. A standard implementation of the edge-detection algorithm suggested by Canny (1986) is used to find the points on the edge of a rod sufficiently contrasted from its surroundings, as shown in Fig. 3b. Once the positions of the edge pixels of the rod in question are known, a least-squares fit of an ellipse to its edge pixels (Halír and Flusser, 1998) is used to find the shape and orientation of the projection of the rod in the camera plane (Fig. 3c). The n_y -component is not directly observable, but can be computed from n_x and n_z if the length of the rod is known.

Estimating the rod length. It is impossible to tell the length of the rod from the length of its projected image in a single frame. However, the rod spends a significant amount of time aligned with the flow in the x - z -plane, where the projected length corresponds to the rod length. We therefore recorded time series of projected rod lengths and computed the distribution of projected rod lengths (Fig. 4). The position of the maximum of the distribution determines

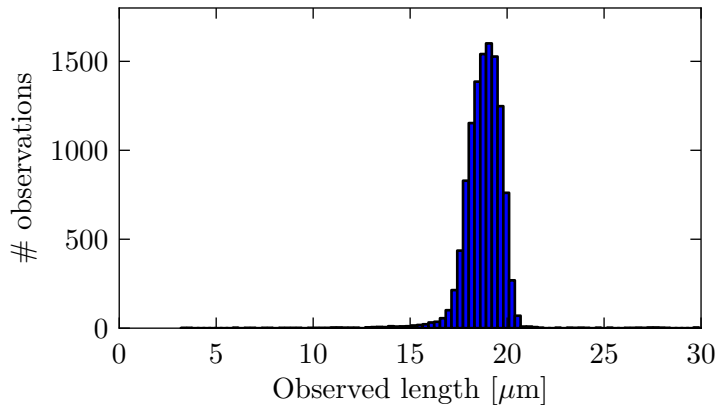


Fig. 4: Histogram of observed projected rod lengths in the x - z -plane following a single particle through the flow. The rod spends a long time nearly aligned with the flow direction. This results in the peak of the histogram. The tail to the left corresponds to observations while the rod is turning around, producing a shorter projection in the camera plane. The peak is broadened by measurement noise due to the finite resolution of the camera. The rod length is taken to be the position of the peak. Data corresponds to rod #1 (see Section 3).

the rod length. We note, however, that the empirical histogram is subject to noise (as a result of the finite resolution of the microscope). This may cause a bias in our estimate of the length.

2.2.2 Time rescaling

As explained above, we revert the flow direction in order to test the sensitivity of observed orientational motion to perturbations. We have found that small perturbations may have significant effects. It is therefore important to revert the flow as smoothly as possible. This means that the flow velocity changes substantially over a significant amount of time. Another source of changes in flow speed u_x is noise in the form of uncontrolled pressure fluctuations in the pump.

But as long as the flow is governed by the linear Stokes equation (as it is in our case), the only effect of fluctuations of u_x is a linear change of time scale. To account for this change, we plot orientational trajectories as a function of distance d along the trajectory of the rod (and not as a function of time t):

$$d(t) = \int_0^t dt' u_x(t'). \quad (2)$$

The instantaneous flow velocity u_x is estimated by the centre-of-mass velocity. We assume, in other words, that the centre-of-mass of the rod is advected

by the channel flow. The change of variables (2) greatly simplifies the analysis of our results.

3 Results

In order to determine the sensitivity of the orientational motion, we record it in the following way. We first track a rod from one end of the channel to the other, recording the centre-of-mass position and orientation of the rod. Then we reverse the flow direction smoothly by reverting the applied pressure difference. In Stokes' equation this turns u_x to $-u_x$ and, by Eq. (2), d to $-d$, effectively reversing time. In an ideal and noise-free experiment the centre-of-mass and orientation are expected to retrace their trajectories. In reality, of course, we observe deviations which allow us to quantify the sensitivity of the observed dynamics to perturbations.

Our results are summarised in Figs. 5 to 7. The data shown in the three figures were obtained for three different rods. Each figure contains three panels: (a) a high-resolution plot of the centre-of-mass trajectory exhibiting small fluctuations Δz in the z -direction, (b) the n_x -component of the orientation vector, before reversal (solid line), and after reversal (dashed line), and (c) the n_z -component of the orientation vector.

Consider first Figure. 5. Panel (a) shows that the fluctuations Δz of the centre-of-mass trajectory are very small, only on the order of $10\ \mu\text{m}$. This is less than one particle length, and is much smaller than the channel width ($2500\ \mu\text{m}$). Panel (b) shows n_x , the component of orientation vector along the flow direction. The particle spends most of its time aligned with the flow, but regularly tumbles between $n_x = 1$ and $n_x = -1$. Upon reversal, the orientational trajectory is initially similar, but drifts out of phase after several flips. The z -component of the orientation vector in panel (c) is, of course, close to $n_z = 0$ while the particle is aligned along the flow. However, during a flip the values of n_z determine which particular orientational path the rod takes. We see that the shape of the n_z -curve during flips is similar for several subsequent flips. This indicates that the orientational trajectory is approximately periodic.

Fig. 6 shows a second example. It is similar to Fig. 5, but corresponds to a different orientational trajectory. The other main difference is that the period time of the tumbling motion is shorter.

Fig. 7 shows an orientational trajectory that exhibits large deviations after reverting the flow. The orientational motion is at first retraced, but after the rod has retraced a full flip, deviations in the orientational motion become noticeable and continue to grow rapidly.

4 Discussion

Figs. 5 to 7 show both translational and orientational trajectories of rods advected in a channel flow. The translational trajectories indicate that the experiment is successfully controlled: the rods stay on straight streamlines during the whole experiment in Figs. 5 to 7. On a finer scale we see that

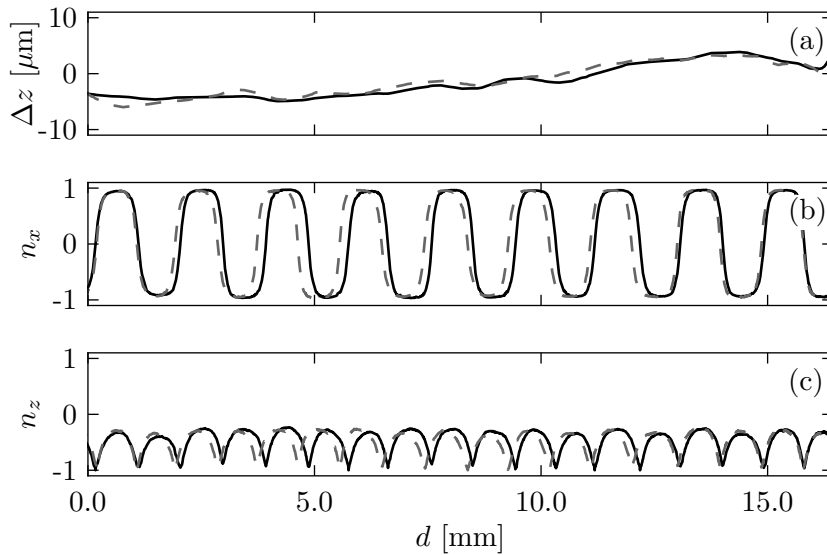


Fig. 5: (a) Fluctuations Δz of the z -coordinate of the centre-of-mass position of a rod advected in the microchannel flow from left to right (solid black line), reversed flow (dashed black line). Here d denotes the distance covered in the x -direction, see Eq. (2). (b) n_x -component of orientation vector. (c) n_z -component of orientation vector. Rod #1 (length $19\ \mu\text{m}$, see Fig. 4).

the streamline followed by the centre-of-mass is slightly curved, on the order of $10\ \mu\text{m}$. This is probably due to imperfections in the channel walls. After reversal, the center-of-mass trajectories of the rods follow the streamlines very well, with only minor fluctuations on the order of one micrometer.

Our main results are the orientational trajectories of the rods shown in Figs. 5 to 7. As expected we observe tumbling motion, and the results include both periodic tumbling (Figs. 5,6) and aperiodic tumbling (Fig. 7). Different realisations of the experiment result in different tumbling periods. Moreover, we observe a weak phase drift between trajectories before and after reversal.

We discuss these observations by first briefly recalling the hydrodynamic Jeffery (1922) theory and its implications for both axisymmetric and triaxial rods. Small axisymmetric rods suspended in a shear flow tumble periodically. More precisely, the orientation vector follows one of infinitely many possible periodic Jeffery orbits. Which particular orbit the rod takes is determined by its initial orientation. For most Jeffery orbits, the rod tumbles: it stays aligned with the streamline for most of the time, but at times it rapidly flips by 180 degrees. When the initial orientation of the rod is very close to the vorticity direction, the tumbling is less pronounced. The corresponding type

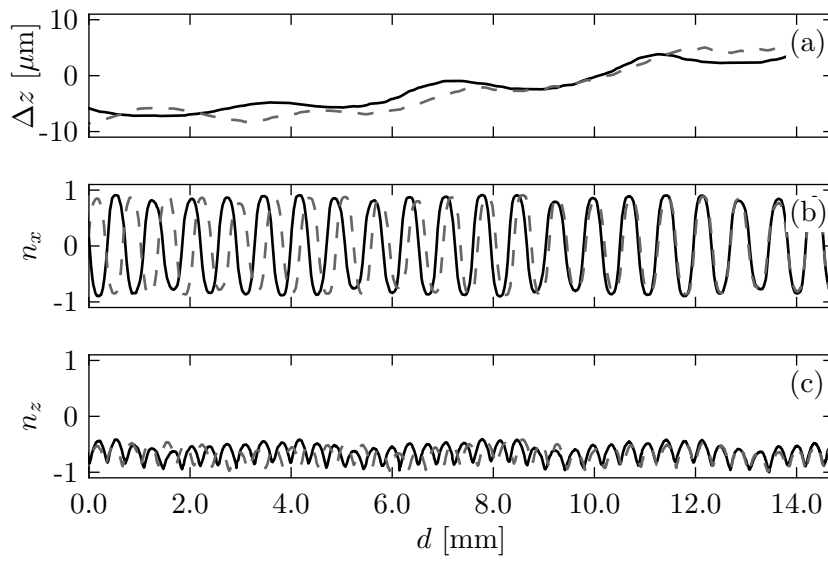


Fig. 6: Same as Fig. 5 but for rod #2 (length $22 \mu\text{m}$).

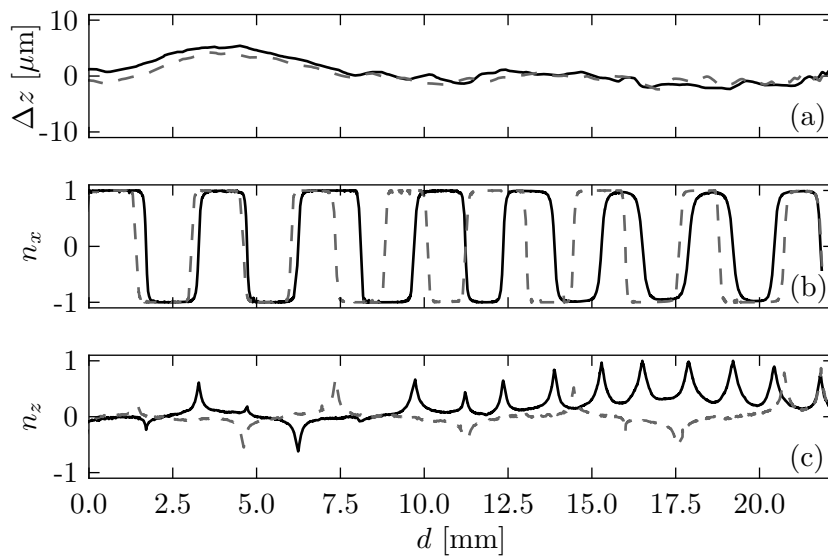


Fig. 7: Same as Fig. 5 but for rod #3 (length $30 \mu\text{m}$).

of orientational motion is often referred to as “kayaking” in the literature, owing to its similarity to the motion of a kayak paddle.

For Jeffery orbits, the tumbling period does not depend on the initial orientation of the rod. The period for a rod of aspect ratio λ suspended in a shear flow of strength s is given by

$$T_{\text{Jeffery}} = \pi \frac{\lambda^2 + 1}{s\lambda}. \quad (3)$$

As mentioned in the introduction, asymmetric particles also tumble, but not necessarily in a periodic fashion (Hinch and Leal, 1979; Yarin et al., 1997).

We begin the discussion of Figs. 5 to 7 by noting two consequences of Eq. (3). First, this equation shows that the different tumbling periods in Figs. 5 and 6 can result from differences in aspect ratio or shear strength: larger aspect ratios correspond to longer periods, stronger shear to shorter periods. The lengths of the particles shown in Figs. 5 and 6 are approximately the same. But the resolution of our microscope does not allow us to precisely determine the thickness of the two rods. We cannot exclude that the different tumbling periods are in part caused by different aspect ratios of the two particles.

Second, we discuss the phase drift between the forward and backward orientational trajectories seen in Figs. 5 and 6 in terms of Eq. (3). We argue that the phase drift is due to fluctuations in the shear that are caused by small fluctuations of the y -coordinate of the centre-of-mass position. As explained in Sec. 2.1, the shear is a function of the y -coordinate. If we assume that the centre-of-mass drift in y is similar in magnitude to that in z (on the order of a few micrometers), we can find a lower bound for the expected phase drift as follows. According to Eq. (3), the period is inversely proportional to the shear strength. It follows that the relative change in shear strength equals the relative change in time between flips, $\Delta s/s = \Delta T/T$. The flow profile in the y -direction is approximately a quadratic function, $u_x = -\alpha y^2$, which implies that $\Delta T/T = \Delta y/y$. Equating y with the channel depth (400 μm) allows us to estimate that the drift should be at least 1%, in agreement with panels (b) and (c) in Figs. 5 and 6.

We conclude the discussion by examining the trajectory in Fig. 7. We see, first, that the trajectory is clearly aperiodic, both before and after reversal. The numerical experiments by Yarin et al. (1997) indicate that triaxial rods may exhibit aperiodic dynamics even for very small deviations from axisymmetry (that could not be resolved by our microscope). Secondly, the forward and backward orientational trajectories in panel (c) of Fig. 7 separate rapidly. In fact, the trajectory appears at first to reverse perfectly but then the difference between forward and backward orientational trajectories grows substantially. These observations suggest that Fig. 7 corresponds to chaotic tumbling of a triaxial particle.

5 Conclusions

We have designed a microfluidic setup with video microscopy and tracking software to measure the translational and orientational trajectories of micro-

rods advected in microchannel flows. The experiments presented here demonstrate the level of control and accuracy of the current setup. We observe both periodic and aperiodic (and possibly chaotic) orientational dynamics.

Further work on the experiment aims to improve the efficiency and capability of the current setup. For example, we plan to install an optical tweezer in order to control initial orientations of the rods. This would make it possible to observe different orientational behaviours (such as those shown in Figs. 5 and 7) for *the same* rod.

Acknowledgements Financial support from the Swedish Research Council and the Göran Gustafsson Foundation for Research in Natural Sciences and Medicine is gratefully acknowledged.

References

- Alargova, R., Bhatt, K., Paunov, V., Velev, O., 2004. Scalable synthesis of a new class of polymer microrods by a liquid-liquid dispersion technique. *Advanced Materials* 16 (18), 1653–1657.
- Bezuglyy, V., Mehlig, B., Wilkinson, M., 2010. Poincaré indices of rheoscopic visualisations. *Europhysics Letters* 89 (3), 34003.
- Brody, J., Yager, P., Goldstein, R., Austin, R., 1996. Biotechnology at low Reynolds numbers. *Biophysical Journal* 71 (6), 3430–3441.
- Canny, J., 1986. A computational approach to edge detection. *Pattern Analysis and Machine Intelligence, IEEE Transactions on PAMI-8* (6), 679–698.
- Cheng, N.-S., 2008. Formula for the viscosity of a glycerol-water mixture. *Industrial & Engineering Chemistry Research* 47 (9), 3285–3288.
- Goldsmith, H., Mason, S., 1962. The flow of suspensions through tubes. i. single spheres, rods, and discs. *Journal of Colloid Science* 17 (5), 448–476.
- Halír, R., Flusser, J., 1998. Numerically stable direct least-squares fitting of ellipses. In: *Proceedings of the 6th International Conference in Central Europe on Computer Graphics and Visualization*. pp. 125–132.
- Hinch, E. J., Leal, L. G., 1972. The effect of Brownian motion on the rheological properties of a suspension of non-spherical particles. *Journal of Fluid Mechanics* 52 (04), 683–712.
- Hinch, E. J., Leal, L. G., 1979. Rotation of small non-axisymmetric particles in a simple shear flow. *Journal of Fluid Mechanics* 92 (03), 591–607.
- Jeffery, G. B., 1922. The motion of ellipsoidal particles immersed in a viscous fluid. *Proceedings of the Royal Society of London. Series A* 102 (715), 161–179.
- Kaya, T., Koser, H., 2009. Characterization of hydrodynamic surface interactions of *Escherichia coli* cell bodies in shear flow. *Phys. Rev. Lett.* 103, 138103.
- Mishra, Y. N., Einarsson, J., John, O. A., Andersson, P., Mehlig, B., Hanstorp, D., 2012. A microfluidic device for the study of the orientational dynamics of microrods. Vol. 8251. SPIE, p. 825109.
- Ott, E., 1993. *Chaos in Dynamical Systems*. Cambridge University Press.
- Parsa, S., Calzavarini, E., Toschi, F., Voth, G. A., 2012. Rotation rate of rods in turbulent fluid flow. *Phys. Rev. Lett.* 109, 134601.

-
- Petrie, C. J., 1999. The rheology of fibre suspensions. *Journal of Non-Newtonian Fluid Mechanics* 87 (2-3), 369 – 402.
- Wilkinson, M., Bezuglyy, V., Mehlig, B., 2009. Fingerprints of random flows? *Physics of Fluids* 21 (4), 043304.
- Wilkinson, M., Bezuglyy, V., Mehlig, B., 2011. Emergent order in rheoscopic swirls. *Journal of Fluid Mechanics* 667, 158–187.
- Wilkinson, M., Kennard, H. R., 2012. A model for alignment between microscopic rods and vorticity. arXiv:1205.6968.
- Yarin, A., Gottlieb, O., Roisman, I., 1997. Chaotic rotation of triaxial ellipsoids in simple shear flow. *Journal of Fluid Mechanics* 340, 83–100.